Experimental Generation of Continuous-Variable Hyperentanglement in an Optical Parametric Oscillator

Kui Liu, Jun Guo, Chunxiao Cai, Shuaifeng Guo, and Jiangrui Gao*
State Key Laboratory of Quantum Optics and Quantum Optics Devices, Institute of Opto-Electronics, Shanxi University, Taiyuan 030006, China
(Received 27 January 2014; published 20 October 2014)

We report on the generation of continuous-variable hyperentanglement of polarization and orbital angular momentum with a type II optical parametric oscillator. By compensating for the astigmatism between spatial modes, we produce an entangled pair of Hermite-Gauss beams. From correlations measurements, we verify the existence of continuous-variable hyperentanglement by the general entanglement criterion as well as by the continuous-variable version of the Peres-Horodecki criterion visualized on an equivalent Poincaré sphere.

DOI: 10.1103/PhysRevLett.113.170501 PACS numbers: 03.67.Bg, 42.50.-p, 42.65.Yj

Entanglement, one of the most striking characteristics of quantum mechanics, plays a significant role in quantum information processing, computation, and communication [1,2]. Recently, much research has been devoted to hyperentanglement, in which the quantum states are simultaneously entangled with more than 1 degree of freedom. In general, optical implementations of quantum information processing benefit from improved manipulation of the different photonic degrees of freedom [2–4]. Studies on various instances of hyperentanglement sources with discrete variables have been motivated by the increased information carrying capacity of such paired photons [5–9]. These hyperentanglement sources have been used to form the building blocks of quantum computation [10,11].

The quantum information science applying both discrete variables of single photons and continuous variables (CVs) of optical modes has developed rapidly. However, CV hyperentanglement has not so far been experimentally explored. Although the applications of CV hyperentanglement have not been discussed extensively, as for the discrete version, this type of entanglement is possible to be used in the multichannel and high-density CV information coding [12] to improve the information capacity. Recently, Coutinho dos Santos *et al.* [13] theoretically predicted CV hyperentanglement in spin angular momentum (SAM) and orbital angular momentum (OAM), which has the potential to be utilized in quantum imaging [14] and quantum metrology to estimate simultaneously the physical parameters more than one, such as spin [15], phase [16], and magnetic field [17]. Another promising application is to implement the CV information transformation on the interface between bright light and atomic ensembles [18].

The SAM of light is associated with its polarization. Korolkova *et al.* [19] introduced the concept of CV polarization entanglement and proposed its generation method. Then Bowen *et al.* [20] first obtained the CV polarization entangled states based on applying vacuum squeezed states and bright coherent states of light. The OAM of light is associated with the transverse spatial distribution of the optical beam, such as Laguerre-Gaussian (LG) modes [21]. A scheme for the generation of OAM CV entanglement has been proposed by Hsu *et al.* [22], and CV entanglement between the two first-order LG modes and OAM squeezing on the orbital Poincare sphere has also been experimentally demonstrated with a spatially nondegenerate optical parametric oscillator (OPO) by Lassen *et al.* [23].

In this Letter, we experimentally demonstrate the simultaneous generation of two pairs of entanglement of first-order Hermite–Gauss modes (HG_{01} entangled states and HG_{10} entangled states) in a type II OPO. We also confirm that the entanglement is the CV hyperentanglement of SAM and OAM.

The Hamiltonian for a type II OPO with OAM is expressed by [13,24]

$$\hat{H} = i\hbar\varepsilon_p(\hat{a}_p^\dagger - \hat{a}_p) + i\hbar\chi(\hat{a}_p\hat{a}_{i,+1}^\dagger\hat{a}_{s,-1}^\dagger - \hat{a}_p\hat{a}_{i,-1}^\dagger\hat{a}_{s,+1}^\dagger) + \text{H.c.} \quad (1)$$

Here $\hat{a}_p$ and $\hat{a}_{j,l}$ are annihilation operators in the Heisenberg picture describing the intracavity pump field and fundamental fields ($j = i, s$: polarization of the LG mode, $l = \pm 1$: OAM of the LG mode), respectively. ε_p is the pump parameter that is proportional to the external pump amplitude, and χ is the strength of the nonlinear coupling of the optical fields.

According to the Hamiltonian of a type II OPO with OAM, the two down-converted fields are in the orthogonal linear polarizations (idler i and signal s) and opposite helical OAM to meet the conservation of energy and OAM. Once a pump photon in a Gaussian mode is annihilated in the down-conversion process, there are two distinct possible channels in which a pair of down-converted photons are created. The two possibilities are (i) an idler photon is emitted in the LG_0^1 mode and a signal photon is emitted in the LG_0^{-1} mode, and (ii) a signal photon is emitted in the LG_0^1

mode and an idler photon is emitted in the LG_0^{-1} mode. Therefore, SAM (polarization) entanglement and OAM mode entanglement are able to be generated in a type II OPO with OAM. Because of the overlap of LG_0^1 and LG_0^{-1} modes in space and time, both HG_{01} and HG_{10} modes appear in the output of the OPO, and they are also entangled.

The experimental setup is depicted in Fig. 1. The 1080-nm laser beam transmits through a three-mirror ring cavity that tailors the spatial profile of the beam to the HG_{01} mode. The 1080-nm HG_{01} laser beam with 45° polarization is injected into the OPO as the seed beam, and the 540 nm laser beam in Gaussian mode with the horizontal polarization is used for the pump field to drive the OPO.

The OPO cavity consists of two mirrors with a radius of curvature of 30 mm ($M1$ and $M2$ in Fig. 1). The piezo-actuated mirror $M1$ (having high reflectivity at 540 and 1080 nm) is used as the input coupler, and mirror $M2$ (having transmission of 4.2% at 1080 nm and an antireflection coating at 540 nm) is used as the output coupler of the entangled beams at 1080 nm.

In general, four modes (idler $HG_{i,01}$, signal $HG_{s,01}$, idler $HG_{i,10}$, signal $HG_{s,10}$) are not able to simultaneously resonate in the OPO cavity owing to the existence of the astigmatic effect [25]. To achieve four modes simultaneously resonating in the cavity, a pair of α-cut type II KTP (potassium titanyl phosphate) crystals and a half-wave plate for Gouy-phase compensation are placed in the OPO, as shown in Fig. 1(b). The pair of α-cut type II KTP crystals ($3 \times 3 \times 10$ mm) are oriented to make their Z axes be perpendicular to each other, and the temperatures of the two crystals are independently controlled. A half-wave plate for a wavelength of 1080 nm is inserted between the two crystals, and its optical axis is rotated 45° relative to the Z axis of the crystal.

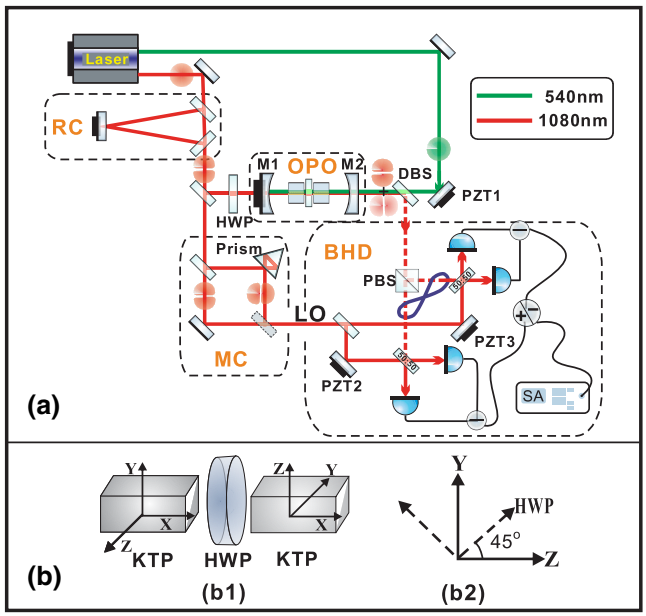

FIG. 1 (color online). Experimental setup. Three-mirror ring cavity (RC), dichroic beam splitter (DBS), polarizing beam splitter (PBS), half-wave plate (HWP), piezoelectric element for controlling phases (PZT), LO, mode converter for the generation of the LO of the HG_{10} mode from the HG_{01} mode (MC), spectrum analyzer (SA), balanced homodyne detectors (BHD). (b1) Placement of the KTP crystals in the OPO. x, y, and z are the axes of the KTP crystal; half-wave plate (HWP). (b2) The 45° angles between the crystal axes [(Y, Z), solid lines] and the optical axes of the half-wave plate (dashed lines).

When we lock the relative phase between the pump field and the injected seed beam in the state of deamplification with PZT1, two types of copropagating (HG_{01} and HG_{10}) entanglement are generated. Using a dichroic beam splitter, the entangled beams are separated from the pump light. In this case, we get two pairs of entangled states, which are the bright entangled HG_{01} optical beams and the HG_{10} vacuum-entangled states. The output entangled beams are divided by the polarizing beam splitter into two parts with orthogonal polarizations, and each part includes both HG_{01} and HG_{10} modes. Then they are analyzed by the balanced homodyne detectors with a spatially tailored local oscillator (LO), which is tailored for measuring either HG_{01} or HG_{10} mode. The LO phases relative to the output beams are controlled by PZT2 and PZT3. When the relative phase is controlled at $\pi/2$ or 0, the noise of the phase quadrature or the amplitude quadrature is measured, respectively.

As shown in Fig. 2(a), we measured the correlation noise of HG_{01} mode normalized to the shot noise limit (SNL) (trace 2) at the analysis frequency of 6 MHz with resolution bandwidth of 1 MHz and video bandwidth of 300 Hz. Figure 2(a1) shows squeezing of -0.56 ± 0.16 dB for the sum of amplitude quadratures (quantum anticorrelation) $\langle \Delta^2(X_{i,H01} + X_{s,H01}) \rangle$ (trace 1) and antisqueezing of 1.20 ± 0.15 dB for the difference of amplitude quadratures $\langle \Delta^2(X_{i,H01} - X_{s,H01}) \rangle$ (trace 3). Figure 2(a2) shows squeezing of -0.76 ± 0.13 dB for the difference of phase quadratures (quantum correlation) $\langle \Delta^2(P_{i,H01} - P_{s,H01}) \rangle$ (trace 1) and antisqueezing of 1.16 ± 0.15 dB for the sum of phase quadratures $\langle \Delta^2(P_{i,H01} + P_{s,H01}) \rangle$ (trace 3). The small difference between the sum and difference (quantum correlation and anticorrelation) is due to the existence of the additional noises. The additional noises derive from the additional noises on the input seed beam and the pump light as well as the extra noise produced in the nonlinear process [26]. Some additional noise is eliminated due to the subtraction of phase quadratures. According to the criterion of Duan *et al.* [27] and Simon [28], we have

$$\langle \Delta^2(X_{i,H01} + X_{s,H01}) \rangle + \langle \Delta^2(P_{i,H01} - P_{s,H01}) \rangle = 1.72 \pm 0.06 < 2, \quad (2)$$

which clearly shows entanglement between the signal and idler of the HG_{01} mode.

Adjusting the LO beam to HG_{10} mode, we measured the entanglement of HG_{10} modes at the analysis frequency of 6 MHz as shown in Fig. 2(b), where trace 2 is the SNL. Figure 2(b1) shows squeezing of -0.68 ± 0.13 dB for the sum of amplitude quadratures $\langle \Delta^2(X_{i,H10} + X_{s,H10}) \rangle$ (trace 1)

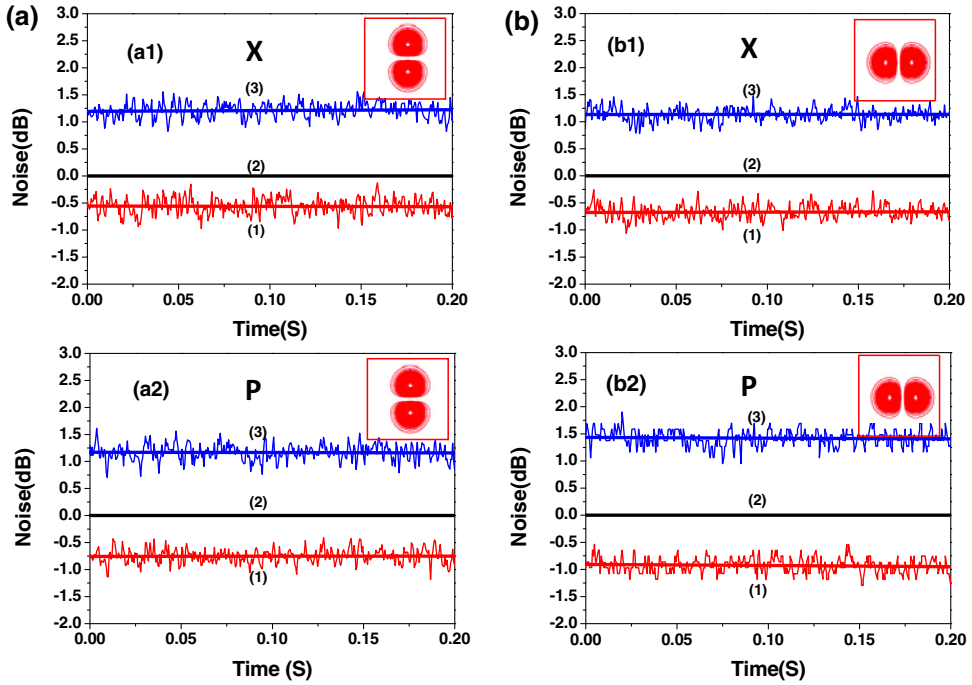

FIG. 2 (color online). Experimental results of entanglement. (a) The correlation noise of HG_{01} modes. (b) The correlation noise of HG_{10} modes. (a1) Trace 1 (red line): $\langle\Delta^2(X_{i,H01}+X_{s,H01})\rangle$; trace 3 (blue line): $\langle\Delta^2(X_{i,H01}-X_{s,H01})\rangle$. (a2) Trace 1 (red line): $\langle\Delta^2(P_{i,H01}-P_{s,H01})\rangle$; trace 3 (blue line): $(\langle\Delta^2(P_{i,H01}+P_{s,H01})\rangle$. (b1) Trace 1 (red line): $\langle\Delta^2(X_{i,H10}+X_{s,H10})\rangle$; trace 3 (blue line): $\langle\Delta^2(X_{i,H10}-X_{s,H10})\rangle$. (b2) Trace 1 (red line): $\langle\Delta^2(P_{i,H10}-P_{s,H10})\rangle$; trace 3 (blue line): $\langle\Delta^2(P_{i,H10}+P_{s,H10})\rangle$. Trace 2 (black line): SNL.

and antisqueezing of 1.13 ± 0.13 dB for the difference of amplitude quadratures $\langle\Delta^2(X_{i,H10}-X_{s,H10})\rangle$ (trace 3). Figure 2(b2) shows squeezing of -0.92 ± 0.14 dB for the difference of phase quadratures $\langle\Delta^2(P_{i,H10}-P_{s,H10})\rangle$ (trace 1) and antisqueezing of 1.42 ± 0.15 dB for the sum of phase quadratures $\langle\Delta^2(P_{i,H10}+P_{s,H10})\rangle$ (trace 3). Thus, we have

$$\langle\Delta^2(X_{i,H10}+X_{s,H10})\rangle+\langle\Delta^2(P_{i,H10}-P_{s,H10})\rangle = 1.67\pm0.06<2, \quad (3)$$

which proves the entanglement between the two HG_{10} modes.

The measured correlations are degraded by the various inefficiencies in the measuring process. The total measuring efficiency should be $\eta_{\rm tol}=\eta_{\rm tr}\eta_{\rm det}\eta_{\rm hd}$, where $\eta_{\rm tr}=0.89\pm0.02$ is the transmitting efficiency, $\eta_{\rm det}=0.90\pm0.03$ is the measuring efficiency of the photodiode (ETX500), and $\eta_{\rm hd}=0.88\pm0.02$ is the spatial overlap efficiency between the signal and LO on the homodyne detector both for HG_{01} and HG_{10} modes. Since the measuring efficiency for the total detection is $\eta_{\rm tol}=0.70\pm0.05$, the inferred entanglement for HG_{01} [Eq. (2)] and HG_{10} [Eq. (3)] are 1.60 ± 0.10 and 1.53 ± 0.11, respectively.

By performing a simple basis transformation from the HG modes to LG modes, it is easy to show that $X_l=\sum_j(X_{j,H01}\mp P_{j,H10})/\sqrt{2}$ and $P_l=\sum_j(P_{j,H01}\pm X_{j,H10})/\sqrt{2}$ $(j=i,s;\ l=\pm1)$; here $\hat{a}_l=(X_l+iP_l)/\sqrt{2}$ represents the LG mode. The entanglement criterion between two OAM modes $\hat{a}_{+1}$ & $\hat{a}_{-1}$ is

$$\langle\Delta^2(X_{+1}+X_{-1})\rangle+\langle\Delta^2(P_{+1}-P_{-1})\rangle=1.69\pm0.06<2. \quad (4)$$

It means that the output of the OPO is OAM entangled. The inferred entanglement criterion value is 1.55 ± 0.06.

Considering the entanglement of two spins (polarizations) $\hat{a}_i$ & $\hat{a}_s$ (signal and idler) in the OPO output, we have

$$\langle\Delta^2(X_i+X_s)\rangle+\langle\Delta^2(P_i-P_s)\rangle=1.70\pm0.06<2; \quad (5)$$

here $X_j=(X_{j,H01}+X_{j,H10})/\sqrt{2}$ and $P_j=(P_{j,H01}+P_{j,H10})/\sqrt{2}$ $(j=i,s)$.

The output of the OPO is also a SAM entanglement state, and the inferred criterion value is 1.57 ± 0.11, which demonstrates the hyperentanglement of SAM and OAM.

The Stokes operators acting on a Poincaré sphere for the first-order OAM modes and SAM modes are denoted by $\hat{O}_k$ [21,22] and $\hat{S}_k$ [19,20] $(k=1,2,3)$, respectively, where

$$\begin{aligned}\hat{O}_1&=\hat{a}^\dagger_{HG10}\hat{a}_{HG10}-\hat{a}^\dagger_{HG01}\hat{a}_{HG01}\\ \hat{O}_2&=\hat{a}^\dagger_{HG10(45^\circ)}\hat{a}_{HG10(45^\circ)}-\hat{a}^\dagger_{HG10(135^\circ)}\hat{a}_{HG10(135^\circ)}\\ \hat{O}_3&=\hat{a}^\dagger_{+1}\hat{a}_{+1}-\hat{a}^\dagger_{-1}\hat{a}_{-1},\end{aligned} \quad (6)$$

$$\begin{aligned}\hat{S}_1&=\hat{a}^\dagger_H\hat{a}_H-\hat{a}^\dagger_V\hat{a}_V\\ \hat{S}_2&=\hat{a}^\dagger_{H(45^\circ)}\hat{a}_{H(45^\circ)}-\hat{a}^\dagger_{H(135^\circ)}\hat{a}_{H(135^\circ)}\\ \hat{S}_3&=\hat{a}^\dagger_R\hat{a}_R-\hat{a}^\dagger_L\hat{a}_L.\end{aligned} \quad (7)$$

$\hat{O}_1$, $\hat{O}_2$, and $\hat{O}_3$ represent the differences of the photon number between the pairs of spatial modes HG_{10} and HG_{01}, $HG_{10(45°)}$ and $HG_{10(135°)}$, and LG_0^1 and LG_0^{-1}, respectively. $\hat{S}_1$, $\hat{S}_2$, and $\hat{S}_3$ represent the differences of the photon number between horizontally (H) and vertically (V) polarized modes, 45° and 135° linearly polarized modes, and right-circularly (R) and left-circularly (L) polarized modes, respectively.

In our setup, the output states of beams s and i both reside in the negative $\hat{O}_1$ region of the orbital Poincaré sphere [Fig. 3(a1)] because of the bright excitation of HG_{01} and the dark HG_{10}. On the spin Poincaré sphere, the beam i resides in the positive $\hat{S}_1$ region [Fig. 3(b1)], whereas the beam s resides in the negative $\hat{S}_1$ region [Fig. 3(b2)] because beam i has horizontal polarization and beam s has vertical polarization.

The fluctuations of Stokes operators of the two output beams (i, s) are then given by

$$\begin{aligned}\Delta\hat{O}_{j,1} &= -2\alpha_{j,HG01}\Delta X_{j,HG01}\\ \Delta\hat{O}_{j,2} &= 2\alpha_{j,HG01}\Delta X_{j,HG10}\\ \Delta\hat{O}_{j,3} &= 2\alpha_{j,HG01}\Delta P_{j,HG10}\,(j=i,s),\end{aligned} \tag{8}$$

$$\begin{aligned}\Delta\hat{S}_{i,1} &= 2\alpha_i\Delta X_i\\ \Delta\hat{S}_{i,2} &= 2\alpha_i\Delta X_{\nu,s}\\ \Delta\hat{S}_{i,3} &= 2\alpha_i\Delta P_{\nu,s},\end{aligned} \tag{9}$$

$$\begin{aligned}\Delta\hat{S}_{s,1} &= -2\alpha_s\Delta X_s\\ \Delta\hat{S}_{s,2} &= 2\alpha_s\Delta X_{\nu,i}\\ \Delta\hat{S}_{s,3} &= 2\alpha_s\Delta P_{\nu,i},\end{aligned} \tag{10}$$

where $\hat{a}_{\nu,j} = (X_{v,j} + iP_{v,j})/\sqrt{2}\,(j = i, s)$ are vacuum fields. According to the measurement, the noise volume of the output beam i (s) is ball shaped [Fig. 3(a2)] on the orbital Poincaré sphere, and the noise levels of all the three OAM Stokes variables are above the SNL. The noise volume of output beam i (s) is cigar shaped [Fig. 3(b3)] on the spin Poincaré sphere, and the noise of $\hat{S}_1$ is above the SNL and the noise levels of $\hat{S}_2$ and $\hat{S}_3$ overlap with the SNL.

In accordance with the definition of relevant variance [19], $V_\pm(\hat{O}_{i,k}, \hat{O}_{s,k}) = \Delta^2(\hat{O}_{i,k} \pm \hat{O}_{s,k})/\Delta^2(\hat{O}_{i,k}^{\rm coh} + \hat{O}_{s,k}^{\rm coh})$, if $V_\pm < 1$, there is quantum correlation between the uncertainties of the Stokes operators. From Eq. (8), we infer that $V_+(\hat{O}_{i,1}, \hat{O}_{s,1}) = 0.82 \pm 0.05$, $V_+(\hat{O}_{i,2}, \hat{O}_{s,2}) = 0.79 \pm 0.05$, and $V_-(\hat{O}_{i,3}, \hat{O}_{s,3}) = 0.73 \pm 0.06$. In other words, after the measurement of beam s, the conditional states of beam i are projected into a cigar-shaped uncertainty volume on the orbital Poincaré sphere, as shown in Figs. 3(a3) and 3(a4). $\hat{O}_1$ and $\hat{O}_3$ or $\hat{O}_2$ and $\hat{O}_3$ can simultaneously be below the SNL. In fact, the CV version of the Peres-Horodecki criterion is the nonseparability criterion of entanglement, which are [19]

$$\begin{aligned}V_+(\hat{O}_{i,1}, \hat{O}_{s,1}) + V_-(\hat{O}_{i,3}, \hat{O}_{s,3}) &= 1.55 \pm 0.10 < 2\\ V_+(\hat{O}_{i,2}, \hat{O}_{s,2}) + V_-(\hat{O}_{i,3}, \hat{O}_{s,3}) &= 1.62 \pm 0.11 < 2.\end{aligned} \tag{11}$$

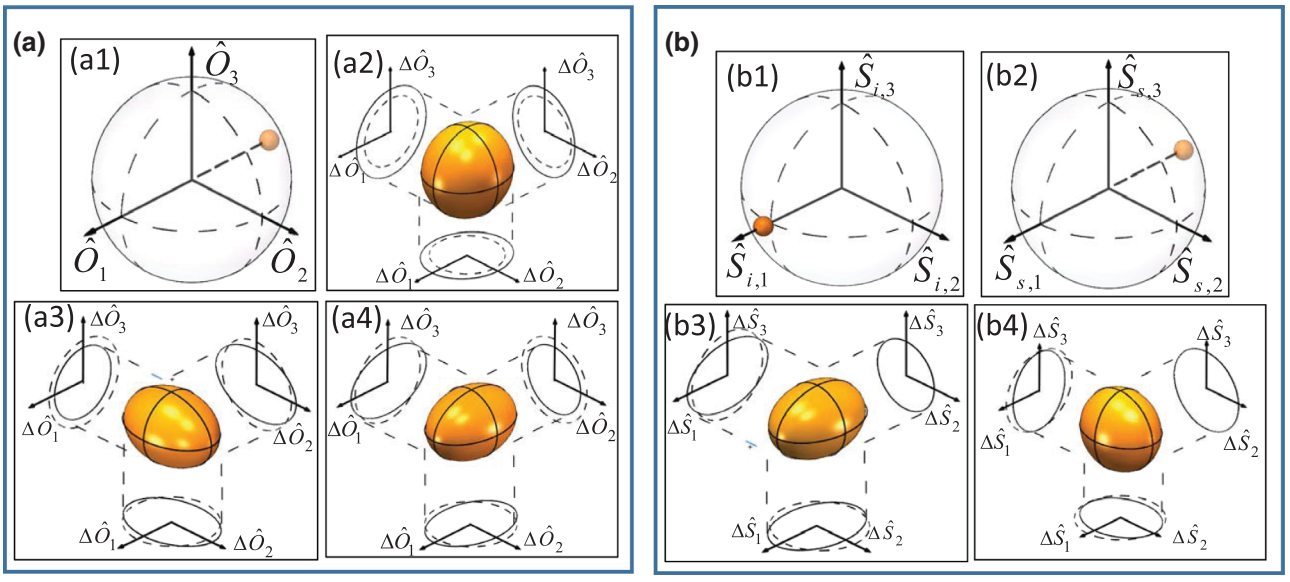

FIG. 3 (color online). Entanglement descriptions mapped on Poincaré spheres. (a) OAM. (a1) Location of output beams on the orbital Poincaré sphere. (a2) Noise volume of beam i before any measurement of beam s. (a3) and (a4) Conditional knowledge of beam i given measurements of $\hat{O}_1$ & $\hat{O}_3$ and $\hat{O}_2$ & $\hat{O}_3$, respectively, on beam s. (b) SAM. (a1) and (a2) Locations of output beams i and s, respectively, on the spin Poincaré sphere. (a3) Noise volume of beam i before any measurement of beam s. (a4) Conditional knowledge of beam i given measurements of $\hat{O}_1$ on beam s. The dashed circles show the SNL. If the conditional knowledge is better than the dashed circles, the states are entangled.

In analogy to the case for OAM, the relevant variances of SAM are $V_+(\hat{S}_{i,1}, \hat{S}_{s,1}) = 0.81 \pm 0.05$, $V_\pm(\hat{S}_{i,2}, \hat{S}_{s,2}) = 1$, and $V_\pm(\hat{S}_{i,3}, \hat{S}_{s,3}) = 1$. In other words, after the measurement of beam s, the conditional noise volume of beam i becomes pie shaped, and only the noise is squeezed to the level below the SNL since the quantum correlation only exists between $\hat{S}_{i,1}$ and $\hat{S}_{s,1}$ [Fig. 3(b4)]. The Peres-Horodecki criteria for SAM are

$$V_+(\hat{S}_{i,1}, \hat{S}_{s,1}) + V_-(\hat{S}_{i,2}, \hat{S}_{s,2}) = 1.81 \pm 0.05 < 2$$
$$V_+(\hat{S}_{i,1}, \hat{S}_{s,1}) + V_-(\hat{S}_{i,3}, \hat{S}_{s,3}) = 1.81 \pm 0.05 < 2. \quad (12)$$

From the above results, the existence of the entanglement on the orbital and spin Poincaré spheres has been demonstrated. Additionally, according to another stricter sufficient but not necessary criterion of entanglement for OAM [22] and SAM [20], there is OAM entanglement ($I(\hat{O}_2, \hat{O}_3) = 0.84 \pm 0.06 < 1$) but no SAM entanglement because our experimental setup does not include a bright coherent beam [20].

We have simultaneously produced two pairs of entanglements of Hermite-Gauss modes (HG_{01} entangled states and HG_{10} entangled states) with a type II OPO and demonstrated that the entanglement is a CV hyperentanglement of SAM and OAM. By characterizing the variances of the Stokes parameters the existence of the hyperentanglement is confirmed. The presented experimental system and scheme provide an efficient way for preparing multipair entanglement. Combining with multipixel homodyne detection, the system is able to be applied in the practical optical multimode and multichannel quantum communication systems. The hyperentanglement is easy to be extended to two-dimensional spatial entanglement [29], which has potential applications in two-dimensional imaging of a tiny particle or a living cell [30] and the tracing measurement of motion beyond the quantum limit [31]. Another promising application of the CV hyperentanglement is to build an interface between light and atoms [32,33] and to realize the high-fidelity quantum memory [34,35].

We thank Professor K. C. Peng, Professor C. D. Xie, and Professor Hans-A. Bachor for helpful discussions. This research was supported by the National Basic Research Program of China (Grant No. 2010CB923102), National Natural Science Foundation of China Project for Excellent Research Team (Grant No. 61121064), and National Natural Science Foundation of China (Grants No. 11274212 and No. 11174189).

*jrgao@sxu.edu.cn

[1] D. Bouwmeester, A. Ekert, and A. Zeilinger, *The Physics of Quantum Information* (Springer-Verlag, Berlin, 2000).
[2] N. J. Cerf, G. Leuchs, and E. S. Polzik, *Quantum Information with Continuous Variables of Atoms and Light* (Imperial College Press, London, 2007).
[3] P. Kok, K. Nemoto, T. C. Ralph, J. P. Dowling, and G. J. Milburn, Rev. Mod. Phys. **79**, 135 (2007).
[4] J.-W. Pan, Z.-B. Chen, C.-Y. Lu, H. Weinfurter, A. Zeilinger, and M. Żukowski, Rev. Mod. Phys. **84**, 777 (2012).
[5] P. G. Kwiat, J. Mod. Opt. **44**, 2173 (1997).
[6] J. Barreiro, N. Langford, N. Peters, and P. Kwiat, Phys. Rev. Lett. **95**, 260501 (2005).
[7] J. Chen, J. Fan, M. Eisaman, and A. Migdall, Phys. Rev. A **77**, 053812 (2008).
[8] G. Vallone, R. Ceccarelli, F. De Martini, and P. Mataloni, Phys. Rev. A **79**, 030301(R) (2009).
[9] R. Ceccarelli, G. Vallone, F. De Martini, P. Mataloni, and A. Cabello, Phys. Rev. Lett. **103**, 160401 (2009).
[10] K. Chen, C.-M. Li, Q. Zhang, Y.-A. Chen, A. Goebel, S. Chen, A. Mair, and J.-W. Pan, Phys. Rev. Lett. **99**, 120503 (2007).
[11] W.-B. Gao, P. Xu, X.-C. Yao, O. Gühne, A. Cabello, C.-Y. Lu, C.-Z. Peng, Z.-B. Chen, and J.-W. Pan, Phys. Rev. Lett. **104**, 020501 (2010).
[12] M. Lassen, V. Delaubert, J. Janousek, K. Wagner, H.-A. Bachor, P. Lam, N. Treps, P. Buchhave, C. Fabre, and C. Harb, Phys. Rev. Lett. **98**, 083602 (2007).
[13] B. dos Santos, K. Dechoum, and A. Khoury, Phys. Rev. Lett. **103**, 230503 (2009).
[14] M. I. Kolobov, *Quantum Imaging* (Springer, New York, 2007).
[15] M. P. J. Lavery, F. C. Speirits, S. M. Barnett, and M. J. Padgett, Science **341**, 537 (2013).
[16] F. Tamburini, G. Anzolin, G. Umbriaco, A. Bianchini, and C. Barbieri, Phys. Rev. Lett. **97**, 163903 (2006).
[17] F. Wolfgramm, A. Cerè, F. A. Beduini, A. Predojević, M. Koschorreck, and M. W. Mitchell, Phys. Rev. Lett. **105**, 053601 (2010).
[18] J. P. Torres and L. Torner, *Twisted Photons: Applications of Light with Orbital Angular Momentum* (Wiley-VCH, Weinheim, 2011).
[19] N. Korolkova, G. Leuchs, R. Loudon, T. C. Ralph, and C. Silberhorn, Phys. Rev. A **65**, 052306 (2002).
[20] W. P. Bowen, N. Treps, R. Schnabel, and P. Koy Lam, Phys. Rev. Lett. **89**, 253601 (2002).
[21] M. J. Padgett and J. Courtial, Opt. Lett. **24**, 430 (1999).
[22] M. Hsu, W. Bowen, and P. Lam, Phys. Rev. A **79**, 043825 (2009).
[23] M. Lassen, G. Leuchs, and U. Andersen, Phys. Rev. Lett. **102**, 163602 (2009).
[24] C. Navarrete–Benlloch, E. Roldán, and G. de Valcárcel, Phys. Rev. Lett. **100**, 203601 (2008).
[25] M. Martinelli, J. Huguenin, P. Nussenzveig, and A. Khoury, Phys. Rev. A **70**, 013812 (2004).
[26] J. César, A. Coelho, K. Cassemiro, A. Villar, M. Lassen, P. Nussenzveig, and M. Martinelli, Phys. Rev. A **79**, 063816 (2009).
[27] L.-M. Duan, G. Giedke, J. I. Cirac, and P. Zoller, Phys. Rev. Lett. **84**, 2722 (2000).
[28] R. Simon, Phys. Rev. Lett. **84**, 2726 (2000).
[29] K. Wagner, J. Janousek, V. Delaubert, H. Zou, C. Harb, N. Treps, J. F. Morizur, P. K. Lam, and H. A. Bachor, Science **321**, 541 (2008).
[30] M. A. Taylor, J. Janousek, V. Daria, J. Knittel, B. Hage, H.-A. Bachor, and W. P. Bowen, Phys. Rev. X **4**, 011017 (2014).
[31] M. A. Taylor, J. Janousek, V. Daria, J. Knittel, B. Hage, H.-A. Bachor, and W. P. Bowen, Nat. Photonics **7**, 229 (2013).
[32] A. Picón, A. Benseny, J. Mompart, J. R. Vázquez de Aldana, L. Plaja, G. F. Calvo, and L. Roso, New J. Phys. **12**, 083053 (2010).
[33] R. Inoue, T. Yonehara, Y. Miyamoto, M. Koashi, and M. Kozuma, Phys. Rev. Lett. **103**, 110503 (2009).
[34] D.-S. Ding, Z.-Y. Zhou, B.-S. Shi, and G.-C. Guo, Nat. Commun. **4**, 2527 (2013).
[35] A. Nicolas, L. Veissier, L. Giner, E. Giacobino, D. Maxein, and J. Laurat, Nat. Photonics **8**, 234 (2014).